Three Dimensional Computational Analysis and Visualization of Worldwide Solar Quiet Daily Variations in the Earth's Magnetic Field

Akinfenwa T. Fashanu, Felix Ale, Olufemi A. Agboola, Babatunde A. Rabiu, Oyewusi Ibidapo-Obe

***Abstract* —** This work develops a high resolution computational platform for visualization and analysis of spatio-temporal profiles of Solar quiet (Sq) daily variation of Earth's magnetic field components. Geomagnetic field data sampled on per minute basis for the year 1996 (a year of solar minimum and beginning of solar cycle # 23 (Rz = 8.6)) was obtained from sixty-four observatory stations of INTERMAGNET global network. Developed computing algorithm and architecture are deployed on high performance computing facility available at the Nigerian Space Agency. Minute by minute Sq values at individual station are evaluated and combined to generate per-minute worldwide maps of Sq daily variation. These maps were sequenced to construct moving images of global daily Sq evolution on a per-minute time scale as demonstrated for the year 1996. Consistent with ionospheric physics; Sq was found steadily maximal at local noon for most locations across the globe. In addition, month-to-month and seasonal variability patterns were observed in Solar quiet along the magnetic North Sq (H). The foci of Sq (H) at different locations on the globe exhibit very high temporal variability. Thus, the developed platform improved time resolution for processing geomagnetic field variations to the scale of sixty seconds. Hence, the developed computational platform supports close monitoring of rapid variations and impulsive changes in Earth's geomagnetic field.

Keywords — Geomagnetic field, Geostatistical interpolation, Ionosphere, Solar quiet daily variations, Solar cycle.

I. Introduction

The Earth's magnetic (or geomagnetic) field (**B**) is a vector quantity that varies in strength and direction with respect to space and time. Campbell [1], used Figure 1 to illustrate how geomagnetic field can be described using combination of three distinct components selected from seven parameters as shown below;

1. Three orthogonal strength components along the East (**X**), true North (**Y**) and vertical (**Z**) directions.
2. The total field (**F**) strength and two anglesof declination (**D**) and inclination (**I**); or
3. Two strength components and an angle, viz, Horizontal (**H**), veritcal (**Z**), declination (**D**)

Akinfenwa T. Fashanu is with the Department of Systems Engineering, Faculty of Engineering, University of Lagos, Yaba, Lagos, Nigeria. (Email: tfashanu@unilag.edu.ng. phone: +2348023263627).

Ale Felix is with Obasanjo Space Centre, National Space Research and Development Agency, Lugbe, Abuja, Nigeria.

Olufemi O. Agboola is with Obasanjo Space Centre, National Space Research and Development Agency, Lugbe, Abuja, Nigeria.

Babatunde A. Rabiu is with Centre for Atmospheric Research, National Space Research and Development Agency, University of Kogi State, Anyigba, Kogi State, Nigeria.

Oyewusi Ibidapo-Obe is with Department of Systems Engineering, Faculty of Engineering, University of Lagos, Yaba, Lagos, Nigeria.

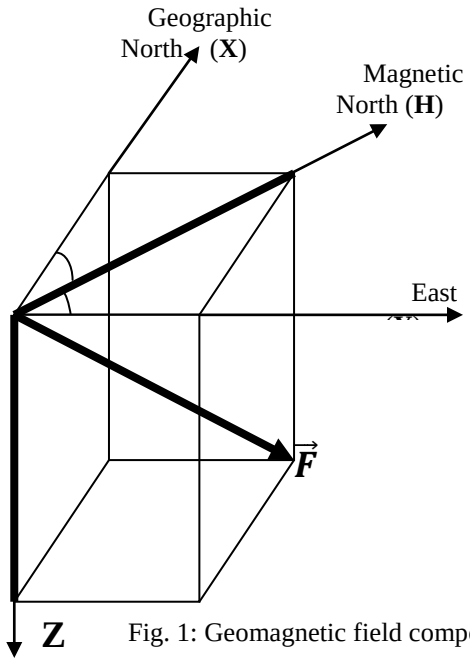

Fig. 1: Geomagnetic field components

Geomagnetic field varies on a wide scale of time scales ranging from milliseconds to millions of years at different location and time. Virginia and co-workers [2] deduced that pattern of geomagnetic field variations also evolves with time. These changes include, slow secular variation that occurs over relatively small time scale of a few to thousands of years. They are due to dynamo processes acting in the Earth's upper atmosphere. Thus, short-term variations are primarily of external origin. They are induced by currents flowing in the ionosphere and magnetosphere [3] [4] [5]. Further studies have established that ionospheric and magnetospheric current systems are jointly responsible for the magnetic field changes on a daily basis. In addition, the ionospheric current in the Earth upper atmosphere is known to be as an outcome of the differential flow of charges caused by solar high energetic particles. According to Ampere's law, this differential flow generates associated magnetic field. Pertubation of the generated field on the main Earth's magnetic field is responsible for the short term variations and can be recorded by ground-based magnetometers.

In effect, currents from solar charged particles flowing in the magnetosphere initiate irregular geomagnetic field variations leading to geomagnetic storms and substorms. Similarly, currents flowing in the ionosphere result into a more or less regular daily variations of the geomagnetic field at both quiet and disturbed conditions.This variation is

known as solar quiet daily variation (Sq). Thus, Sq variations is an index of the ionospheric current system flowing in the dynamo E-region between the altitude of 90 and 130 km which can be demonstrated in 2-D and 3-D forms. The ionospheric current is a charge current which is released by the expansion and contraction of the atmosphere due to worldwide solar winds and tidal forces resulting from diurnal rising and falling of the Sun [6]. The Sq current flow system varies with respect to longitude, latitude and local time of specific geospatial station during quiet and disturbed days [7] [8] .

Technical literature shows that computational analyses of geomagnetic field variations during quiet and disturbed time implemented on regional basis at large time intervals typical of seasons, years, months and days. Hitherto, algorithm development and processing power of computing devices constrained the time step of monitoring solar quiet daily variation to large time-steps; covering a small spatial region of the earth per run [9]. Although, analyses of geomagnetic field variations using conventional large time scales are useful in the study of some geophysical phenomena that may occur over a long time range; obviously, it is inadequate for detailed analyses and investigation of geophysical events that are precipitated in less than an hour. This work therefore presents illustrative computational algorithm and architecture for obtaining Sq daily variation across the globe for solar cycle number 23; using geomagnetic dataset obtained at 1-minute sampling rate.

Given that adverse condition in the ionosphere can initiate disruption of the operations of space- and ground-based technological systems. Some of such systems include satellites, communications signal and networks. Others are GSM/GPS navigations systems, electric power distribution grids, pipelines, ground based control stations. Thus, causal effects of ionospheric disturbances is a basis for scientific research in Space weather monitoring and prediction. In this regard, computational techniques are advancing detailed study of solar quiet daily variations as a means to further understand space weather phenomena [10] [11] [12].

Geomagnetic field data sampled at one-minute rate is useful for a detailed study of rapid impulses, perturbations and variations due to solar radiation. It also facilitates close study of space weather and tracking of geomagnetic phenomena with time scale less an hours. According to [13] , such phenomena include travelling ionospheric disturbance, sky-waves as well as ultra-low frequency waves (ULF) among others. For example, the signature of ULF waves as evident in geomagnetic field variations has been identified as a possible precursor to earthquakes occurrence. Hence, there is need for early and effective warning system that predicts anomalous geophysical phenomena that may have adverse consequences on human and other critical technological systems.

The next section gives a brief description of the techniques employed for computation in this work. Section 3 present the procedure for correcting secular and non-cyclic variations of geomagnetic field and baseline function for each observatory station. Results obtained are presented and discussed in Section 4. A brief summary is presented in Section 5.

II. Materials and Method of Data Analysis

Data acquired and the computational methods deployed for its analysis are presented in this section.

A. The Geomagnetic Field Dataset

Geomagnetic field data was obtained from International Real-Time Magnetic Network (INTERMAGNET). As at 1996, the network consists of sixty four widely distributed observatory stations that were operated by different institutes in twenty countries. Figure 2 shows the spatial distributions of the observatory stations whose data are used in this study.

INTERMAGNET observatory network was selected due to its wide geospatial spread and homogeneous distribution of the measurements on the Earth's surface. The network obtains and collate geomagnetic field data using ground-based digital fluxgate magnetometers which sampled the components of the field vector in X, Y, Z, H, D,Z orientations.

For in-depth analysis, the observatory stations were categorized into low, middle and high latittudes as shown in Table 1. The study of geomagnetic field variation was carried out at quiet condition using the international quiet days (IQD) dataset as well as the geographical coordinate (longitude and latitude) of the observatory stations. The IQDs which are by definition the sets of quiet days per month based on disturbance Kp index were selected and the one-minute values of the components were sampled and quantized to generate the solar quiet daily variation (Sq). According to Australia Geoscience Institute (2016) on solar observatory, IQD are the days when solar activities are relatively quiet while IDD (International Disturbed Days) are disturbed days with very active solar activities. The five

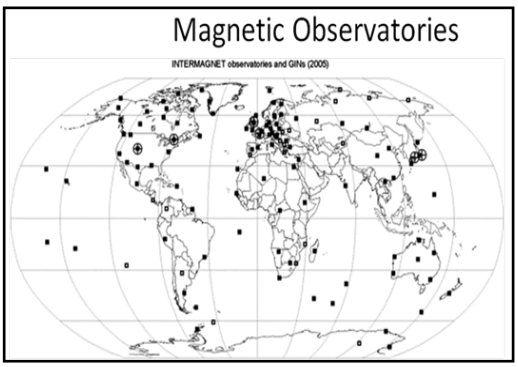

Source: www.intermagnet.org

quietest days of each month were used to compute solar quiet daily variations from the geomagnetic field data for the year 1996.

B. Post-acquisition process

Geomagetic field dataset in IAGA format from 64 ground-based observatories worldwide were sampled on per minute basis and pre-processed using Java script. The dataset was organized in geographic (X,Y,Z,F) and magnetic (H,D,Z,F) planes according to the installed fluxgate sensors orientation. The dataset was pre-processed and compiled in standard format syntactically acceptable for Matlab m-files, scripts, functions and codes.

Table 1: Classification of Observatories According to Latitudes

Station ID	Low Latitude (0-30^0)	Middle Latitude (31-60^0)		High Latitude (60-90^0)
		AMS	HER	ABK
	BNG	BDV	KAK	ALE
	BSC	BEL	LER	BLC
	DLR	BFE	LOV	BRW
	GUA	BOU	MEA	CBB
	HON	CLF	MMB	CMO
	KOU	CNB	NCK	DRV
	MBO	CZT	NEW	IQA
	PHU	ESK	NGK	MBC
	PPT	EYR	NUR	NAQ
	SJG	FCC	OTT	RES
	TAM	FRD	PAF	SBA
	TAN	FRN	PBQ	SOD
		FUR	SIT	THL
		GDH	STJ	YKC
		GLN	THY	
		GNA	TUC	
		HAD	VIC	
			WNG	

Source: www.intermagnet.org

C. Computational Algorithm for Geomagnetic field Data Analysis

For detailed analysis of daily spatio-temporal variations of the geomagnetic field, the acquired dataset was analyzed and converted from geographic to magnetic coordinates using the orthogonal geometric relationship stated in (1) to (4).

From Figure 1, it is clear that

$$F^2 = \mathrm{H}^2 + \mathrm{Z}^2 \quad (1)$$

Where *H* is given by

$$\mathrm{H} = \sqrt{\mathrm{X}^2 + \mathrm{Y}^2} \quad (2)$$

$$X = \mathrm{H} * \mathrm{Cos}(\mathrm{D});\ \mathrm{Y} = \mathrm{H} * \mathrm{Sin}(\mathrm{D}) \quad (3)$$

and

$$D = \arctan(\frac{\mathrm{Y}}{\mathrm{X}}) \quad (4)$$

Solar quiet daily variations along H, D and Z components of geomagnetic field were computed simultaneously. This involves, correction and adjustment of baseline values, mid-night departures and non-cyclic variations using formulae in equations (5) to (11).

According to [14] and [15], these procedures sufficiently filter other sources of geomagnetic field variations that are due to the Earth core and other extraneous magnetic materials on the Earth crust.

The realized baseline values on per minute time basis were used to adjust and correct non-random error in the H, D and Z values so as to enhance their confidence limit. The daily baseline value (M_0) on 1-minute basis is defined as the average for 240 minutes flanking the local midnight at each stations, that is:

$$M_0 = \frac{\sum_{t=1}^{120} M_t + \sum_{t=1324}^{1440} M_t}{240} \quad (5)$$

Where $\mathrm{M_o}$ = baseline values at*t*= 1, 2… 1440 (local time) and $\mathrm{M_t}$ represents Ht, $\mathrm{D_t}$ or $\mathrm{Z_t}$.

At local mid-night, ionospheric current is expected to be minimal due to low solar impact. Thus, minute-by-minute departures of (ΔM_t) from midnight baseline were obtained by subtracting the midnight baseline values of a particular day from all *1-minute* values for that same day as shown in equation 6.

$$\Delta M_t = M_t - M_0 \quad (6)$$

Reference [16] and [15] defined non-cyclic variation as a phenomenon in which the value of (H_t) at 01 local time is different from the value at 1440 local time. Non-cyclic variation due to geomagnetic storm was removed by making linear adjustment in the daily minute values of ΔM_t.as follows:

$$\Delta \boldsymbol{c} = \left(\frac{\Delta \boldsymbol{M_1} - \Delta \boldsymbol{M_{1440}}}{\boldsymbol{1439}}\right) \quad (7)$$

Where **Δc** are mean values of the magnetic elements for two intervals of time in minute. The linear adjustment generates the Sq field as follows:

$$\boldsymbol{Sq} = \Delta \boldsymbol{M_t} + (\boldsymbol{t} - \boldsymbol{1})\Delta \boldsymbol{c} \quad (8)$$

Specifically, we have:

$$\boldsymbol{Sq_H} = \Delta \boldsymbol{H} + (\boldsymbol{t} - \boldsymbol{1})\Delta \boldsymbol{c} \quad (9)$$

$$\boldsymbol{Sq_D} = \Delta \boldsymbol{D} + (\boldsymbol{t} - \boldsymbol{1})\Delta \boldsymbol{c} \quad (10)$$

$$\boldsymbol{Sq_Z} = \Delta \boldsymbol{Z} + (\boldsymbol{t} - \boldsymbol{1})\Delta \boldsymbol{c} \quad (11)$$

The sixty-four stations have three components each in the year 1996 with three hundred and sixty-six days. The diurnal (24-hour) data for H, D, Z-component is equivalent to 1440 minutes. This results to data-intensive computation of 101,191,680 matrix cases (i.e. 3*64*366, 1440). Thus the desired computational visualization and analysis of Sq(H), Sq(D) and Sq(Z) in up to 3-Dimensions require computer hardware with high processing power to generate overall results in a reasonable time.

D. Spatial Data Prediction Using Kriging Algorithm

To proceed, geomagnetic field dataset was approximated evenly over the Earth surface by using Kriging algorithm. The scheme is an efficient geo-statistical interpolation tool suitable for spatial or regionalized variables such as geomagnetic field data, [17] and [18]. The scheme uses enhanced best fit values and corresponding variogram to estimate unobserved values at some grid points using

measured values at other nodes. Processing the geomagnetic field time series data for solar quiet daily variations by Kriging interpolation algorithm was implemented on Matlab m-files with the Matlab parallel computing toolbox. This was implemented on multi-cores systems for effective parallel computations. The framework was in the manner of [19] and [20].

The computation of Sq field used (long-lat, IQD) data, including a field of observed data, the estimated range (time series magnetic data), the resolution of the estimated range (minute (time) resolution data), variogram model. The output is the estimated Sq and error variance. Whereas it is difficult to obtain exhaustive values of geomagnetic field data at every longitude and latitude across the globe due to sparsely located observatories. The kriging spatial interpolation technique was used on observed data to facilitate the analysis of the solar daily quiet variation in dynamic two and three dimensional contour map. The interpolated method used enhanced best fitting values as demonstrated by the variogram estimated 3D contours. The data gridding was carried out using kriging algorithm implemented on Suffer Grid-data in Matlab environment.

Although, geomagnetic field components exhibit spatial continuity, it is not always possible to sample every location of the longitude and latitude. So, unobserved values must be estimated from available observatories data. Sampling and estimation of global variables were done such that the profile of solar quiet daily variation could be mapped and visualized on contour frames from one location to the other across the earth.

E. Procedures for Implementation of Kriging Algorithm

The spatial mean of the geomagnetic data in a stationary condition ($\overline{U}$) and distance between observatories locations were computed using the approach of [18] and [21]. Consequently, data pair *P*(i, j) of the covariance terms were generated by

$$P(\mathrm{i},\mathrm{j}) = \left(\mathrm{U_i} - \overline{\mathrm{U}}\right)\left(\mathrm{U_j} - \overline{\mathrm{U}}\right) \quad (12)$$

$$where\ i = 1,2,\dots,n; and\ j = 1,2,\dots,r.$$

The data pairs were ordered from lower to higher separation distance and grouped. For pairs within a separation rings of distance (r), the covariances of the data is obtained as shown in equation (13);

$$\mathrm{Cov}[\mathrm{U}(\mathrm{X}), \mathrm{U}(\mathrm{X}+\mathrm{r})] = \frac{1}{\mathrm{nr}} \sum_{(\mathrm{i},\mathrm{j})=1}^{\mathrm{nr}} \left(\mathrm{U_i} - \overline{\mathrm{U}}\right)\left(\mathrm{U_j} - \overline{\mathrm{U}}\right) \quad (13)$$

nr is number of data pairs within the ring.

Equation (13) generates a covariance matrix with each data pair *P(i, j)* assigned a value of covariance:

$$\mathrm{C_{i,j}} = \mathrm{Cov}\left(\mathrm{U_i} - \mathrm{U_j}\right) \quad (14)$$

If the covariance of the data is plotted against the separation distance, then we have for each data point (i), the distance between location (i) and the desired Kriging location (o) is obtained. With this distance (i, o), the covariance $C_{i,\,o}$ of each data pair is evaluated using the Kriging equation;

$$\sum_{i=1}^{n} w_i = 1 \quad (15)$$

$$\sum_{j=1}^{n} C_{ij} w_j - \lambda = C_{io} \quad (16)$$

$where\ i = 1,2,\dots,n.\ and\ \lambda$ is the Lagrange multiplier.

Solving this set of (n+1) equations (15) and (16) simultaneously generate the Kriging estimate expressed as:

$$\widehat{U}_o = \sum_{i=1}^{n} w_i U_i \quad (17)$$

The estimation error due to the Kriging algorithm is expressed as;

$$E\left[\left(\widehat{U}_o - U_o\right)^2\right] = \sum_{i=1}^{n}\sum_{j=1}^{n} w_i w_j Cov(U_i, U_j) + \sigma^2 U - 2\sum_{i=1}^{n} w_i Cov(U_i, U_o) \quad (18)$$

Equation (18) can also take the form;

$$E\left[\left(\widehat{U}_o - U_o\right)^2\right] = \sigma^2 U + \sum_{i=1}^{n}\sum_{j=1}^{n} w_i w_j C_{ij} - 2\sum_{i=1}^{n} w_i C_{io} \quad (19)$$

Substituting equation (16) in equation (19) we have;

$$E\left[\left(\widehat{U}_o - U_o\right)^2\right] = \sigma^2 U + \sum_{i=1}^{n} w_i(\lambda + C_{io}) - 2\sum_{i=1}^{n} w_i C_{io} \quad (20)$$

Since $\sum_{i=1}^{n} w_i = 1$ and $E\left[\left(\widehat{U}_o - U_o\right)^2\right] = \sigma^2 k$ i.e. Kriging variance.

Therefore

$$\sigma^2 k = \lambda - \sum_{i=1}^{n} w_i C_{io} \quad (21)$$

Here the Kriging variance is the approximation error due to inconsistent measurement of the geomagnetic field data, uncertainty of λ, and imprecision of spatial data correlation.

III. Results and Discussion

This work applied the Kriging method to analyze worldwide spatio-temporal variations of geomagnetic field and diurnal solar variability at quiet condition. The algorithm was implemented on high performance computers using parallel programming technique. Results are presented as 3-dimensional computational visualization of day-to-day Sq (H), Sq(D) and Sq(Z) variability maps replicating

ionospheric current variations for the year 1996. The 3-dimensional scale include time and locations in terms of longitude and latitude. Figure 3 shows some selected snapshots of Sq(H) variations at different local time across longitudinal and latitudinal zones. On magnetically quiet days, the diurnal geomagnetc field variations occur in smooth and regular form but at the different degrees of latitudes across longitudinal locations and time. These maps revealed that Sq in H and D is greater at daytime than night time and SqH maximizes in daytime at about local noon when the Sun is vertically overhead. In general, at about local noon, Sq in D has strongest focus at latitude below 0°. Unlike Sq(H), Sq(D) does not maintain a consistent maximum along the local noon across the latitudes. Rather, there is variability in the period of maxima with latitudes. It is also apparent that maxima values of Sq(D) drift along latitudes and attain maximum values at the following latitudes with respective solar periods.

In addition, 3D visualization in Figure 3 further shows that Polar Regions exhibits high Sq(H) at local night. The Polar Regions often have high Sq due to consistent solar intensity, even at the night time. This is mainly due to the shape of the Earth and other unknown geophysical activities at the Northern and Southern hemispheres during various seasons of the year. This pattern confirms the contributions of [22] [23] and [24] about additional current system from interplanetary space and specific occurrence of geomagnetic storms in the Polar Regions. Thus, these results further establish the occurrence of seasonal variations of solar activities across the northern and southern hemispheres.

In scope, spatial analysis of geomagnetic field variations is successfully extended from regional to global scale and Sq in three directions (i.e. Sq(H), Sq(D), and Sq(Z)) with one-minute time step for all regions. The amplitude of Sq(H) was higher at the northern pole than the southern pole. This confirms existing results on thermal stability of the southern hemisphere. Sharp geomagnetic spikes are recorded more often in the northern hemisphere to confirm high geophysical activities in the polar region. Generally, Sq(H), Sq(D) and Sq(Z) exhibit significant variability with Sq(H) exhibiting its highest gradient along the equatorial region. This is an index of intense solar activity and ionospheric impact that is consistent with atmospheric dynamo theory.

IV. Conclusion

A high resolution analysis of spatio-temporal variations of geomagnetic field using Kriging method on high performance computing platform has been presented. Implicitly, the study provides a basis for one-minute time scale visualization of the ionospheric current field across the globe. When applied on real time data, this solution can serve as a monitoring system that helps avoid harmful effect of ionospheric current surge on space-borne and other related technological systems. It can also help predict the advent of some natural disasters. The developed computational platform for Sq daily variation can support further research on early detection of travelling ionospheric disturbance (such as typhoon, tsunami etc.) and other related geophysical phenomena.

V. Acknowledgment

The results presented in this paper rely on data collected at magnetic observatories. We thank the national institutes that support them and INTERMAGNET for promoting high standards of magnetic observatory practice (www.intermagnet.org).We are also grateful to National Space Research & Development Agency (NASRDA), Abuja, Nigeria for making available the advanced computing facility for the analysis and simulation of the geomagnetic field dataset.

VI. References

[1] W. H. Campbell, Introduction to Geomagnetic Fields, 1997.

[2] K. Virginia, M. Odim, O. D. Margarete and R. R. P. Andres, "Main patterns of the geomagnetic field: A case study using principal component analysis," 2015.

[3] B. S. Zossi, A. G. Elias and M. Fagre, "Ionospheric Conductance Spatial Distribution During Geomagnetic Field Reversals," *Journal of Geophysical Research: Space Physics*, vol. 123, no. III, p. 2379–2397, 2018.

[4] U. T, Y. K, K. H, Y. A, O. J. V, S. S. I and V. E. F, "Characteristics of energy transfer of Pi 2 magnetic pulsations: Latitudinal dependence," *Geophysical Research Letters*, vol. XXVII, no. 11, pp. 1619-1622, 2000.

[5] N. A. B. Paulo, A. A. Mangalathayil, S. R. Jonas, D. M. Clezio, B. N. F. Paulo, S. d. S. d. C. P. João and S. P. M. Ana, "Latitude-dependent delay in the responses of the equatorial," *annales geophysicae journal*, p. 139–147, 2018.

[6] M. Hagen and A. Azevedo, "Sun-Moon-Earth Interactions, External Factors for Earthquakes," *Natural Science*, vol. IX, pp. 162-180, 2017.

[7] C. Manoj, A. Kuvshinov, S. Maus and H. Lühr, "Ocean circulation generated magnetic signals," *Earth, Planets and Space*, 2006.

[8] W. H. Campbell and E. R. Shiffmacher, "Quiet ionospheric currents and earth conductivity profile computed from the quiet-time geomagnetic field changes in the region of Australia," *Australia journal of physics*, pp. 73-87, 1987.

[9] L. J. Jeffrey and F. A. Carol, "The USGS Geomagnetism Program and Its Role in Space Weather Monitoring," *Space Weather*, 2011.

[10] B. Volker and D. A. Ioannis, Space Weather: Physics and Effects, 2007.

[11] T. Fashanu, F. Ale, A. O. Agboola and O. Obe, "Performance Analysis of a Parallel Computing Algorithm Developed for Space Weather Simulation," *International Journal of Advancements in Research & Technology*, vol. I, no. 7, pp. 46-55, 2012.

[12] F. Ale, O. Ibidapo-Obe, T. A. Fashanu and O. A. Agboola, "Parallel Computation of Spatio-Temporal Variations of Geomagnetic Field Using One-Minute Time Resolution Dataset," vol. 2, no. 11, pp. 1842-1853, 2012.

[13] P. J. Chi and C. T. Russell, "Time domain magnetoseismology: Magnetospheric sounding by timing the tremors in space," *Geophysical Research Letters*, vol. 32, 2005.

[14] F. N. Okeke, C. A. Onwumechili and B. A. Rabiu, "Day-to-day variability of geomagnetic hourly amplitudes at low latitudes," *Geophysical Journal International*, p. 484–500, 1998.

[15] A. Rabiu, "Seasonal variability of solar quiet in middle latitudes," *Ghana Journal of Science*, pp. 15-22, 2005.

[16] E. H. Vestine, Main geomagnetic field. In S. &. Matshushita, Physics of Geomagnetic Phenomena, 1967, pp. 181-234.

[D. G. Krige, "A Statistical Approaches to Some Basic Mine Valuation

17] Problems on the Witwatersrand," *Journal of the Chemical, Metallurgical and Mining Society of South Africa,* pp. 119-139, 1951.

[18] G. Matheron, "Principles of geostatistics," *Economic Geology,* pp. 1246-1266, 1963.

[19] G. Ananth, G. Karypis, K. Vipin and A. Gupta, Introduction to Parallel Computing, 2005.

[20] B. George, D. Rémi, D. Jack and L. Julien, "Algorithm-based fault tolerance applied to high performance computing," *J. Parallel Distrib. Comput.,* p. 410–416, 2009.

[21] D. Dorsel and T. La Breche, "Environmental Sampling and Monitoring Primer: Kriging," 1997.

[22] E. Ilya, L. Jan, B. Dalia, B. H. John and I. Nepomnyashchikh, "Unexpected Southern Hemisphere ionospheric response to geomagnetic storm of 15 August 2015," *Annales Geophysicae,* p. 71–79, 2018.

[23] C. Puethe and A. Kuvshinov, "Towards quantitative assessment of the hazard from space weather. Global 3-D modellings of the electric field induced by a realistic geomagnetic storm," *Earth, Planets, and Space,* pp. 1017-1025, 2013.

[24] G. K. Simi, G. Manju, M. Haridas, S. Nayar, T. Pant and A. Suresh, "Ionospheric response to a geomagnetic storm durfing November 8-10, 2004," *Simi, K & Manju, G & Haridas, Madhav & NAYAR, SRPRABAKARAN & Pant, Tarun & A, Suresh. (2013). Ionospheric response to a geomagnetic storm during November 8-10, 2004. Earth Planets and Space,* pp. 331-336, 2013.

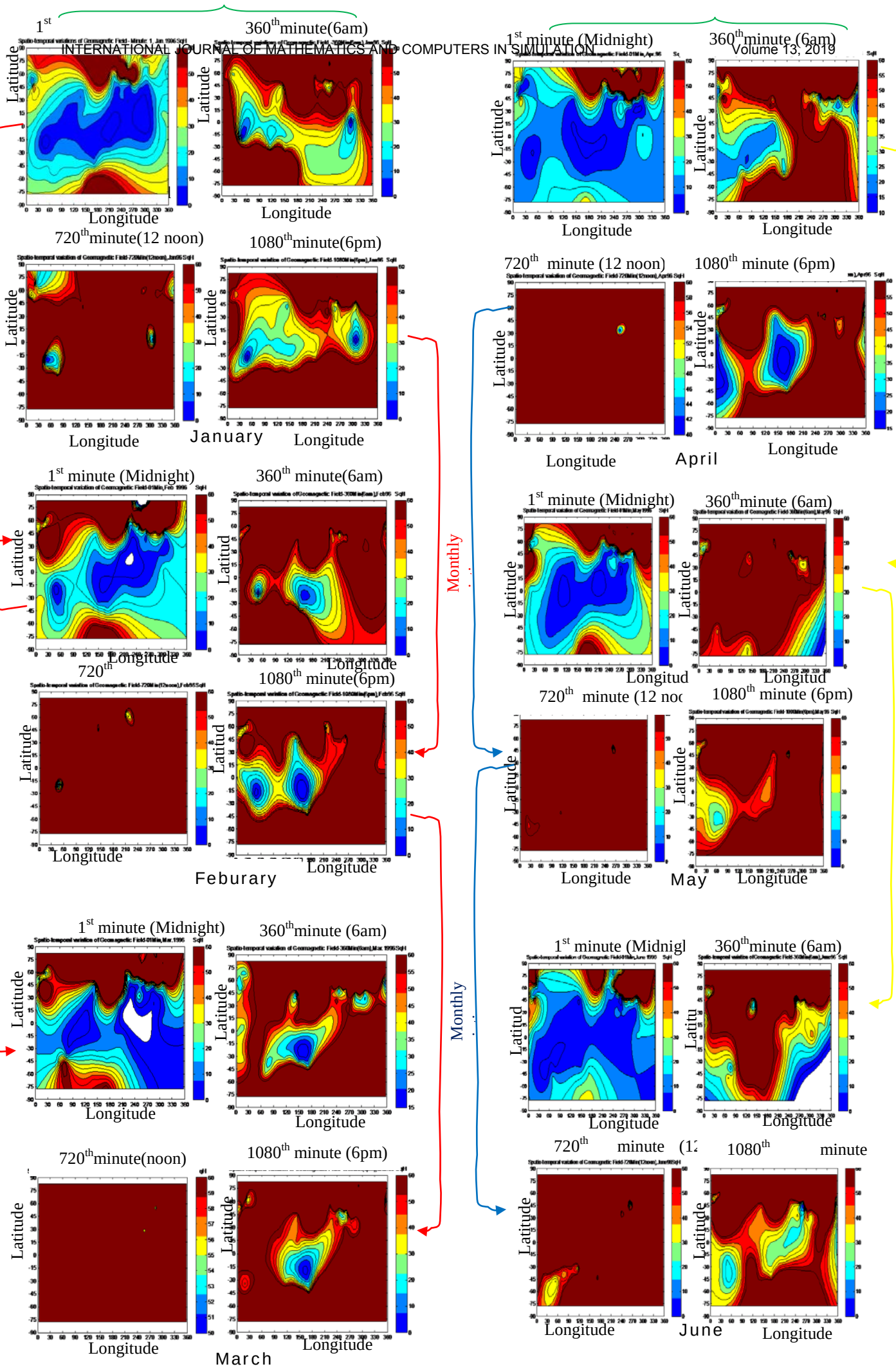
1st
360th minute(6am)
Latitude
Longitude
720th minute(12 noon)
1080th minute(6pm)
January
1st minute (Midnight)
360th minute(6am)
720th minute (12 noon)
1080th minute (6pm)
April
Monthly
Feburary
May
March
June

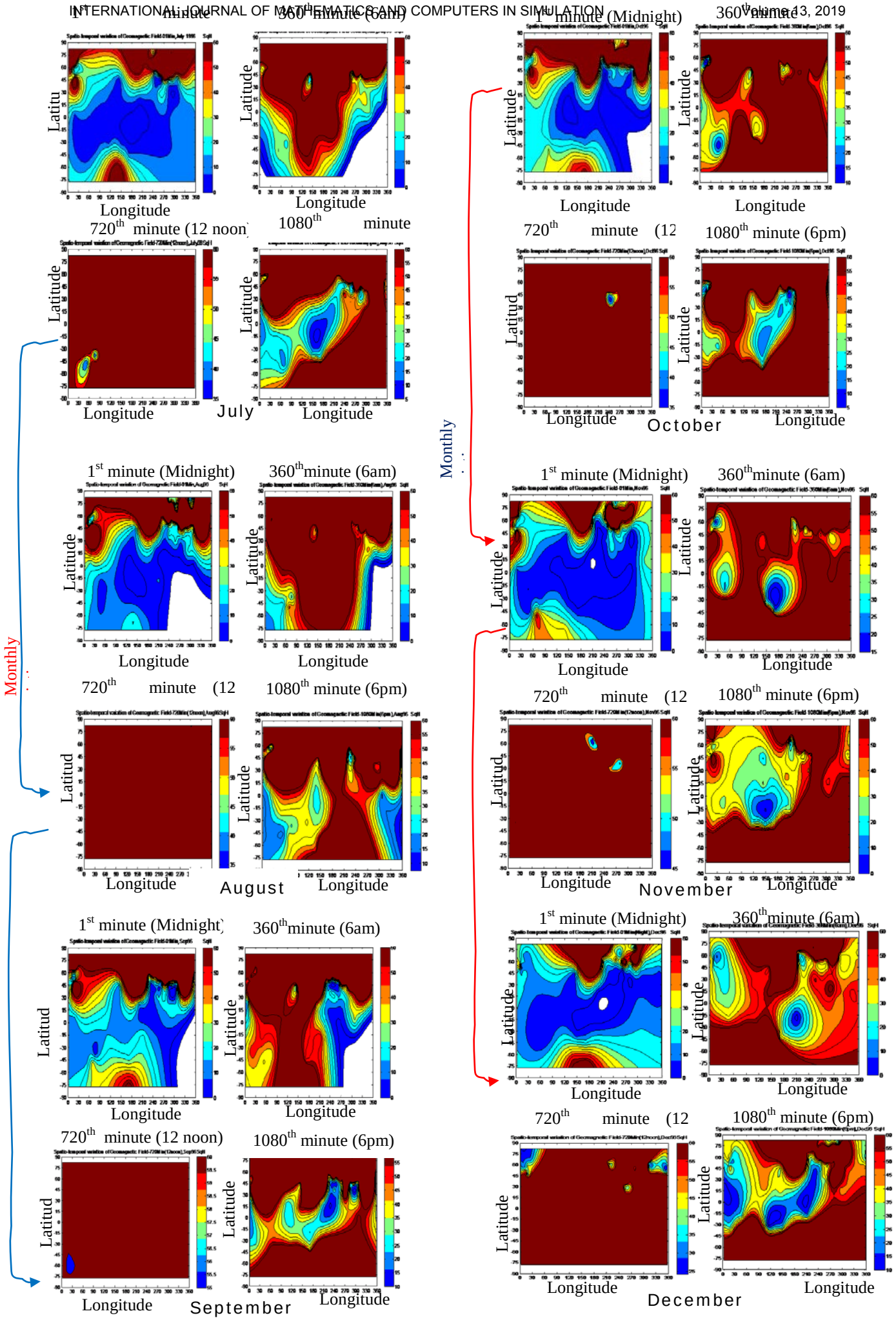

Fig.3: 3-D Visualization of Sq Variations